

## Research Article

# Substrate Temperature-Dependent Structural, Optical, and Electrical Properties of Thermochromic VO<sub>2</sub>(M) Nanostructured Films Grown by a One-Step Pulsed Laser Deposition Process on Smooth Quartz Substrates

Ali Hendaoui 

Physics Department, College of Science and General Studies, Alfaisal University, P.O. Box 50927, Riyadh 11533, Saudi Arabia

Correspondence should be addressed to Ali Hendaoui; [ali.hendaoui@gmail.com](mailto:ali.hendaoui@gmail.com)

Received 11 June 2021; Accepted 27 August 2021; Published 6 September 2021

Academic Editor: Prasenjit Guptasarma

Copyright © 2021 Ali Hendaoui. This is an open access article distributed under the Creative Commons Attribution License, which permits unrestricted use, distribution, and reproduction in any medium, provided the original work is properly cited.

Thermochromic M-phase vanadium dioxide VO<sub>2</sub>(M) films with different morphologies have been grown directly on smooth fused quartz substrates using low deposition rate pulsed laser deposition without posttreatment. When the substrate temperature was increased in the range 450°C–750°C, better (011) texturization of VO<sub>2</sub>(M) films was observed along with an enhancement of their crystallinity. Morphology evolved from small-grained and densely packed VO<sub>2</sub>(M) grains at 450°C to less packed micro/nanowires at 750°C. Mechanisms behind the crystallinity/morphology evolution were discussed and correlated with the effect of the temperature on the diffusion of the adatoms as well as on the V<sup>5+</sup> valence states content in VO<sub>2</sub>(M) films. Resistivity measurements as a function of temperature revealed that the insulator-to-metal transition features of VO<sub>2</sub>(M) films (i.e., transition temperature ( $T_{\text{IMT}}$ ), resistivity variation ( $\Delta R$ ), hysteresis width ( $\Delta H$ ), and transition sharpness ( $\Delta T$ )) are strongly dependent on the processing temperature. In terms of optical properties, it was found that the open (i.e., porous) structure of the films achieved at high temperature induced an improvement of their luminous transmittance. Simultaneously, the enhancement of the films crystallinity with the temperature resulted in better IR modulation ability. The present contribution provides a one-step process to control the morphology of VO<sub>2</sub>(M) films grown on smooth quartz substrates for applications as switches, memory devices, and smart windows.

## 1. Introduction

Thermochromic M-phase Vanadium dioxide VO<sub>2</sub>(M) undergoes an insulator-to-metal transition (IMT) that takes place around a temperature of  $T_{\text{IMT}} \approx 340\text{K}$ . Below  $T_{\text{IMT}}$ , VO<sub>2</sub>(M) has a monoclinic phase characterized by a high resistivity (insulator). Above  $T_{\text{IMT}}$ , VO<sub>2</sub>(M) displays a tetragonal phase with metallic characteristics. The IMT is reversible and takes place at ultrafast timescales and is characterized by a dramatic change in its resistivity as well as in its infrared optical properties from being highly transmissive to being highly reflective, while the optical properties in the visible range remain almost unchanged across  $T_{\text{IMT}}$  [1–3]. This makes VO<sub>2</sub>(M) very promising for ultrafast electronic switching devices, memristors, and smart

windows applications, especially since the critical temperature can be decreased to room temperature by donor-level doping [2]. Full exploitation of the IMT in VO<sub>2</sub>(M) requires a thorough control of its IMT features, such as  $T_{\text{IMT}}$ , hysteresis width  $\Delta H$ , and modulation capability of its electrical and/or optical properties depending on the targeted application. For example, a sensor would require a small hysteresis, sharp transition, and large modulation, while a memristor requires a large hysteresis. It is worth mentioning that the IMT characteristics in VO<sub>2</sub>(M) films depend on their crystallinity and grain morphology, in addition to the impurity/dopants content [4, 5].

Several reports in the literature describe studies on VO<sub>2</sub>(M) with controlled IMT properties for targeted applications [1–8]. Among them, pulsed laser deposition

(PLD) holds a privileged position for the productions of pure  $\text{VO}_2(\text{M})$  thin films with controlled composition, crystallinity, and morphology [2–5]. It has also the potential for large-scale production, especially if the thin films' synthesis is performed at low deposition rates [9]. The crystallinity and morphology of the  $\text{VO}_2(\text{M})$  films can be controlled via several parameters, including the substrate's temperature during the deposition process. By controlling the substrate temperature at  $700^\circ\text{C}$ , in a recent report, Lafane et al. reported the synthesis of  $\text{VO}_2(\text{M})$  polycrystalline nanoplatelets on glass substrate by PLD using Vanadium Pentoxide  $\text{V}_2\text{O}_5$  target under oxygen ambient [10]. However, Lafane et al. did not report information about the composition of the films. In addition, the functional properties of the grown nanoplatelets are not reported therein [10]. In summary, despite the importance of the substrate temperature for controlling the IMT characteristics of PLD-grown nanostructured  $\text{VO}_2(\text{M})$  films, the related studies remain relatively scarce. In addition, the influence of the substrate temperature on the vanadium valence content of the PLD-grown nanostructured  $\text{VO}_2(\text{M})$  films on smooth quartz substrates remains, to the best of our knowledge, unexplored.

Another important topic of interest related to the present study is related to the synthesis of  $\text{VO}_2(\text{M})$  micro/nanowires (MNWs). In fact, many approaches have been developed to achieve  $\text{VO}_2(\text{M})$  MNWs. In most of the cases, the proposed methods resulted in relatively low yield (i.e., surface density) for the micro/nanowires [11, 12]. As a remedial solution, roughening the substrate surface, patterning it, or using epitaxial growth were proposed [11–14]. However, these approaches are either not suitable for optical applications (roughness and patterning), or not applicable for large-scale production (epitaxy). For example, optical applications such as smart windows require large transmittance of the samples in the visible range of the spectrum. In this sense, smooth surface substrates are needed because the presence of roughness or patterns on the substrates surface would negatively impact the optical transmittance. As for the epitaxy, it could be a limiting factor for large scale, that is, commercial production of thin films, since it requires the use of costly single crystalline substrates with atomic-level smoothness and specific lattice characteristics, such as single crystalline titanium dioxide or sapphire substrates for growing  $\text{VO}_2(\text{M})$ , in order to ensure lattice matching between the substrate and the films.

In this paper, we will investigate the influence of the temperature on the composition, structure, and electrical and optical properties of  $\text{VO}_2(\text{M})$  films directly grown on smooth fused quartz substrates by a simple PLD approach at a low deposition rate without posttreatment. Smooth quartz substrates were chosen as they are convenient for resistivity measurements and suitable for optical applications.

We will demonstrate that a control of the substrate temperature of the PLD-grown  $\text{VO}_2(\text{M})$  films allows the control of their IMT features as revealed by resistivity measurement. On the other hand, we will demonstrate that, as the morphology changes from densely packed small grains to less packed micro/nanowires with increasing the temperature, an enhancement of luminous transmittance of

the films is obtained. In addition, we will show that the improvement of  $\text{VO}_2(\text{M})$  crystallinity with the temperature results in an improvement of infrared (IR) transmittance modulation ability toward smart windows applications.

## 2. Materials and Methods

PLD was performed using KrF excimer pulsed laser ( $\lambda = 248 \text{ nm}$ , fluence  $= 1.8 \text{ J}\cdot\text{cm}^{-2}$ ) focused on Vanadium target (99.9% pure) under 5 mTorr of oxygen ambient. Such a low pressure was chosen as it is expected to be beneficial for producing elongated structures due to the enhanced mobility of the adatoms on the substrate. The total number of laser pulses on the target for each deposition experiment was set at 18000 pulses. Smooth fused quartz, used as the substrate, was kept at 7 cm away from the target and the substrate temperature was varied for the different experiments. The laser was pulsed at a frequency of 2 Hz. The choice of this value is based on preliminary tests on the influence of the laser pulsing frequency on the morphology of the grown films toward the synthesis of  $\text{VO}_2(\text{M})$  micro/nanowires. In fact, as shown in Figure S1 on the supplemental file, scanning electron microscope (SEM) images revealed that a pulsing frequency of 2 Hz is suitable for achieving elongated, rods-like structures for  $\text{VO}_2(\text{M})$  grains for films grown at the same substrate temperature.

X-ray photoelectron spectroscopy (XPS) measurements were made using a VG Escalab 220I-XL system with Al  $K\alpha$  ( $h\nu = 1486.6 \text{ eV}$ ) radiation. Etching with Argon was performed for 900-second prior measurements to surface contamination and/or overoxidation. More details about the deconvolution analysis of the binding energy of the  $\text{V}2p_{3/2}$  core level peak to determine the vanadium valence state content of the samples are given in the supplemental file (cf. Figure S2 in the supplemental file).

The crystalline structure of the samples was analyzed by X-ray diffraction (PANalytical's X'Pert, Cu  $K\alpha$  radiation). Their morphology was studied using scanning electron microscopy (JEOL JSM-6300F). The resistivity of the films was measured in the range  $25^\circ\text{C}$ – $100^\circ\text{C}$  using four-point probe. Optical transmittance was analyzed in the range of 250–2500 nm using a spectrophotometer (Agilent, Cary 5000) at normal incidence.

The integral luminous transmittance  $T_{\text{lum}}$  (390–830 nm) and IR transmittance  $T_{\text{IR}}$  (830–2500 nm) were calculated using the following equation:

$$T_{\text{lum/IR}} = \frac{\int \varphi_{\text{lum/IR}}(\lambda) T(\lambda) d\lambda}{\int \varphi_{\text{lum/IR}}(\lambda) d\lambda}, \quad (1)$$

where  $\varphi_{\text{IR}}(\lambda)$  is the IR irradiance spectrum for air mass 1.5 for a  $37^\circ$  tilted surface [15] and  $\varphi_{\text{lum}}(\lambda)$  is the CIE (2008) physiologically relevant luminous efficiency function for photopic vision [16].

The modulation  $\Delta T_{\text{IR}}$  is defined as  $\Delta T_{\text{IR}} = T_{\text{IR,RT}} - T_{\text{IR,90}^\circ\text{C}}$ , where  $T_{\text{IR,RT}}$  and  $T_{\text{IR,90}^\circ\text{C}}$  are, respectively, the integral IR transmittance at room temperature and at  $90^\circ\text{C}$ .

### 3. Results and Discussion

**3.1. Composition Analysis.** Figure 1 shows the evolution of the  $V^{5+}$ ,  $V^{4+}$ , and  $V^{2+}$  valence states content with the substrate temperature extracted from XPS measurements. As can be seen in Figure 1,  $V^{4+}$  is the dominant valence in the sample, which corresponds to the state related to  $VO_2$ .  $V^{4+}$  content decreases in favor of an increase in the  $V^{5+}$  content with increasing the temperature. Therefore, higher oxidation of the films is obtained with increasing the temperature. On the other hand, the content in  $V^{2+}$  remains relatively constant as a function of the temperature as it originates from the creation of oxygen vacancies during the Argon etching process rather than the films PLD synthesis process itself.

**3.2. Microstructure and Morphology Analysis.** Figure 2 shows the XRD patterns of the  $VO_2(M)$  films. All the peaks could be identified using Joint Committee on Powder Diffraction Standards (JCPDS) Card No. 44-0252 and were attributed to  $VO_2(M)$  monoclinic phase. (011) preferred orientation of the films was identified for the peak present at  $\sim 28^\circ$  indicating texturization of  $VO_2(M)$  along the (011) plane as it is the energetically favored one [17, 18]. The preferential crystal growth along the (011) plane is enhanced as the substrate temperature increases from  $450^\circ\text{C}$  to  $750^\circ\text{C}$  as shown by the increase in the (011) peak intensity. The inset in Figure 1 shows that the full width at half maximum (FWHM) of peak (011) decreases with increasing the substrate temperature, indicating an improvement of the crystallinity for the  $VO_2(M)$ .

Figure 3 presents the top-view SEM images of  $VO_2(M)$  films obtained at different substrate temperatures. At  $450^\circ\text{C}$ , the  $VO_2(M)$  film shows a small-grained, densely packed structure due to the relatively low diffusion of adatoms alongside the high nucleation rate that characterizes the PLD process. At  $550^\circ\text{C}$ , the structure displays the coexistence of grains and platelets. The sample synthesized at  $650^\circ\text{C}$  shows the formation of micro/nanorods with well-defined facets and a low aspect ratio.

The evolution of the microstructure and morphology of  $VO_2(M)$  films with varying the processing temperature from  $450^\circ\text{C}$  to  $650^\circ\text{C}$  can be explained by the increase of the diffusion due to a concurrent effect of the temperature and the  $V^{5+}$  content. In fact, increasing the temperature not only improves the diffusion of the ad-atoms but also increases  $V^{5+}$  content in the films. Since  $V^{5+}$  state suggests the existence of  $V_2O_5$ , bulk diffusion is favored due to the low melting temperature of  $V_2O_5$  ( $\sim 680^\circ\text{C}$ ) in accordance with the structural zone model for film growth described by Movchan-Demchishin [19]. More pronounced (011) texturization and better crystallinity of the  $VO_2(M)$  films are obtained as the consequence of enhanced diffusion of the adatoms to grow the planes with the lowest energy [17, 18]. At the same time, the improvement of the diffusion helps in minimizing surface and interface energies by allowing the growth of large grains at the expense of smaller grains.

At  $750^\circ\text{C}$ , the structure of  $VO_2(M)$  changes significantly with the formation of micro/nanowires with a high aspect

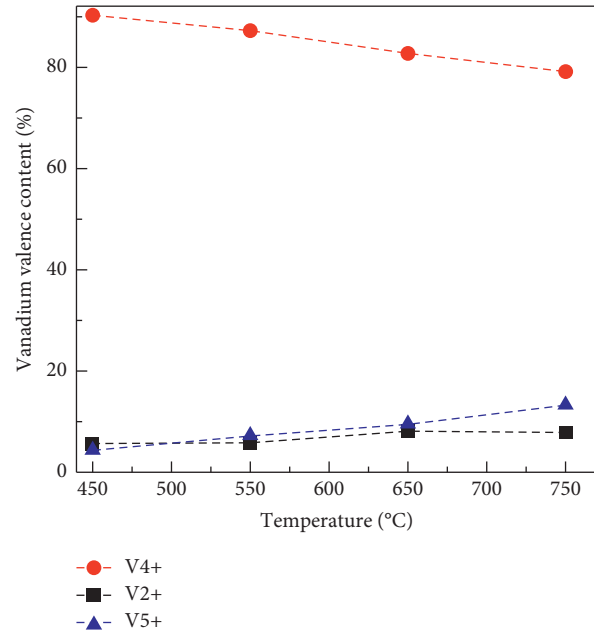


FIGURE 1: Vanadium valence in the PLD-grown  $VO_2(M)$  films.

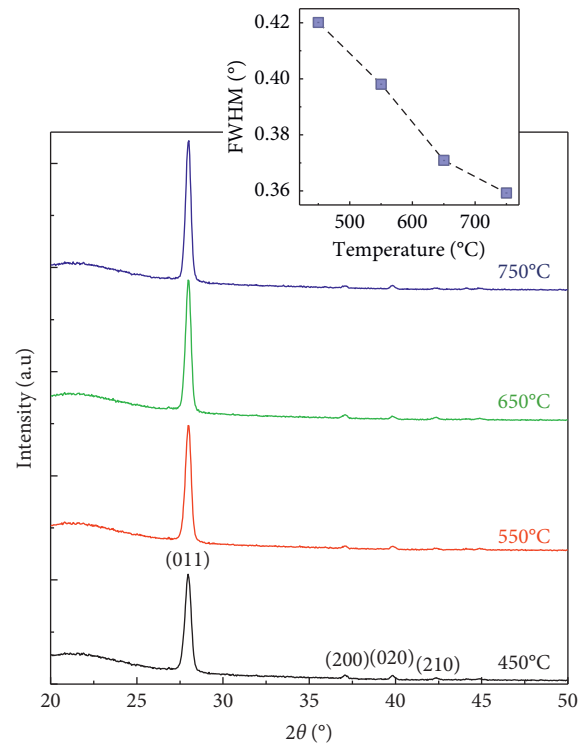


FIGURE 2: XRD patterns of the PLD  $VO_2(M)$  films grown at different temperatures. The inset shows the full width at half maximum (FWHM) of the peak (011) versus growth temperature.

ratio. This temperature is above the melting point of  $V_2O_5$  ( $\sim 680^\circ\text{C}$ ), which can exist as an intermediate liquid phase during the PLD growth of  $VO_2(M)$  structures. The liquid  $V_2O_5$  enhances the formation of micro/nanowires through the wetting assisted growth mechanism, as described by Strelcov et al. [18]. At the same time, the high nucleation rate

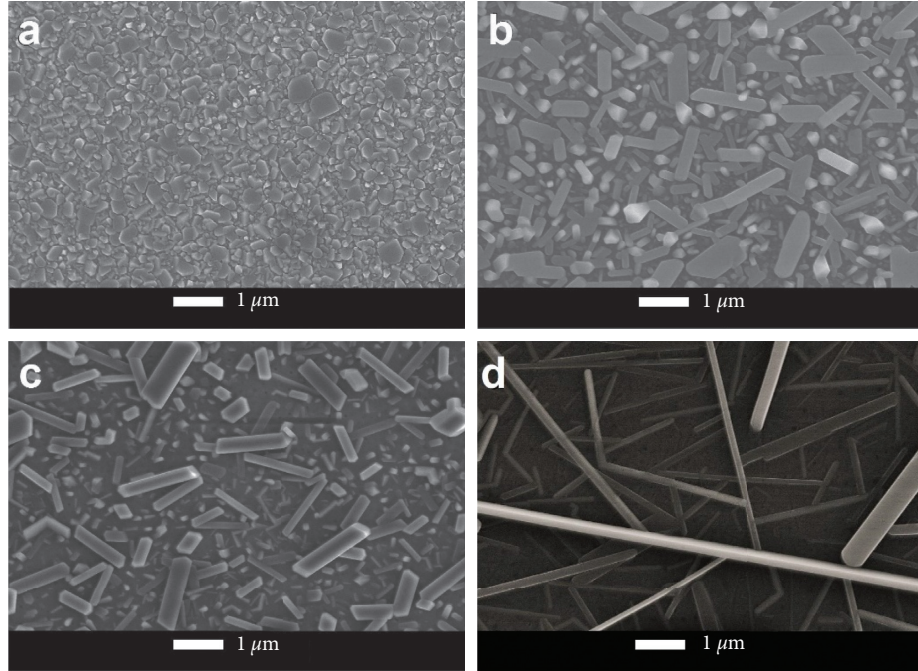


FIGURE 3: SEM images of the PLD  $\text{VO}_2(\text{M})$  films grown at different substrate temperatures: (a) 450°C, (b) 550°C, (c) 650°C, and (d) 750°C.

for the PLD process is beneficial for increasing the surface density (i.e., the yield) of the micro/nanowires on smooth fused quartz substrates, while the high mobility of the PLD adatoms is expected to increase the aspect ratio of the micro/nanowires for a temperature lower than those reported for thermal evaporation-based techniques [20].

**3.3. Electrical Characterization.** The resistivity measurement as a function of the temperature of the  $\text{VO}_2$  samples deposited at  $T = 450^\circ\text{C}$ ,  $550^\circ\text{C}$ , and  $650^\circ\text{C}$  is shown in Figure 4. The resistivity of the film deposited at  $750^\circ\text{C}$  could not be measured as the related values were beyond the upper limit of the four-point probe setup. The increase of the resistivity of the films can be explained by two main reasons: first, high  $\text{V}^{5+}$  content at high temperature is correlated to the existence of excessive oxygen atoms that will induce holes (i.e., acceptor) doping in the  $\text{VO}_2$  films [21]. Second, as the temperature increases, the films become less dense (cf. SEM images in Figure 3), which will further contribute to the increase of their overall resistivity.

The IMT features were obtained from the resistivity curves as follows: the resistivity variation,  $\Delta R$ , is defined as  $\Delta R = \log_{10}(R_{25^\circ\text{C}}/R_{100^\circ\text{C}})$ , where  $R_{25^\circ\text{C}}$  and  $R_{100^\circ\text{C}}$  are the resistivity values at  $25^\circ\text{C}$  and  $100^\circ\text{C}$ , respectively. The first derivative of the resistivity versus temperature was fitted with a Gaussian function (cf. Figure 5). The insulator-to-metal transition temperature ( $T_{\text{IMT}}$ ) is obtained from the position of the minimum of the Gaussian fit of the first derivative of the curve  $\text{resistivity} = f(T)$  for the heating segment, while the hysteresis width ( $\Delta H$ ) is calculated as the difference between the minimum of the Gaussian fit of the first derivative for the heating segment (insulator-to-metal transition) and that for the cooling (metal-to-insulator

transition) segment. Finally, the transition sharpness ( $\Delta T$ ) corresponds to the FWHM of the Gaussian fit curves. The corresponding results are summarized in Table 1.

$T_{\text{IMT}}$  is observed to increase with increasing the substrate temperature (cf. Table 1). This can be explained by the acceptor-level doping of the films due to the increase in the  $\text{V}^{5+}$  valence content that tends to shift  $T_{\text{IMT}}$  to higher values. The largest  $\Delta R$  was achieved for the sample deposited at  $450^\circ\text{C}$  (3.18 orders).  $\Delta R$  decreases with increasing the substrate temperature from  $450^\circ\text{C}$  to  $650^\circ\text{C}$  (cf. Table 1). This result is correlated to the  $\text{V}^{4+}$  content, so that large  $\text{V}^{4+}$  content corresponds to a larger  $\Delta R$ . In parallel, the hysteresis loop  $\Delta H$  increases for samples processed at higher temperature. This can be attributed to the increase of grain size as explained by Suh et al. [22]. Finally, the transition sharpness ( $\Delta T$ ) is known to depend on the type of defects and their concentration in the films as well as on the mechanical stress in the grains of different sizes [4, 22–27]. At low substrate temperature,  $\text{VO}_2(\text{M})$  grains are of a relatively small size and display a low discrepancy in the size (cf. Figure 3(a)). In this case,  $\Delta T$  is low indicating a sharp transition as a result of a low density of bulk defects [4, 23]. In addition, a symmetric hysteresis loop is observed. For  $\text{VO}_2(\text{M})$  films processed at high temperatures, the grain size increases along with the exacerbation of the discrepancy in the grain size (Figures 3(b) and 3(c)). As a result,  $\Delta T$  increases and an asymmetric hysteresis loop is observed due to the more pronounced difference in the values of  $\Delta T$  for the heating and cooling segments of the resistivity curves of the same sample.

**3.4. Optical Properties of the  $\text{VO}_2(\text{M})$  Films toward Smart Windows Application.** Several approaches were reported to improve the properties of  $\text{VO}_2(\text{M})$  for smart windows

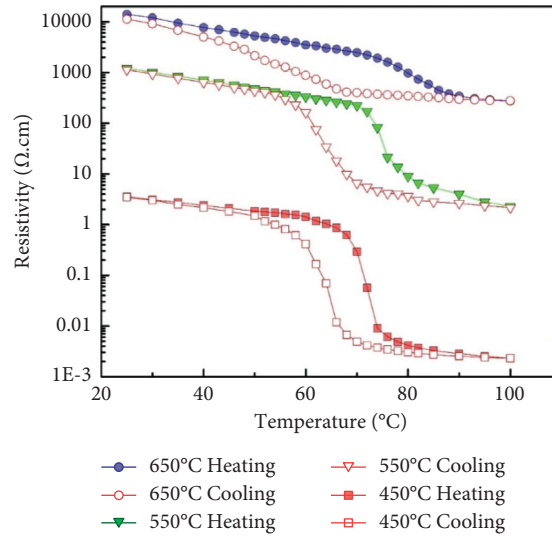


FIGURE 4: Resistivity versus temperature of the PLD VO<sub>2</sub>(M) films.

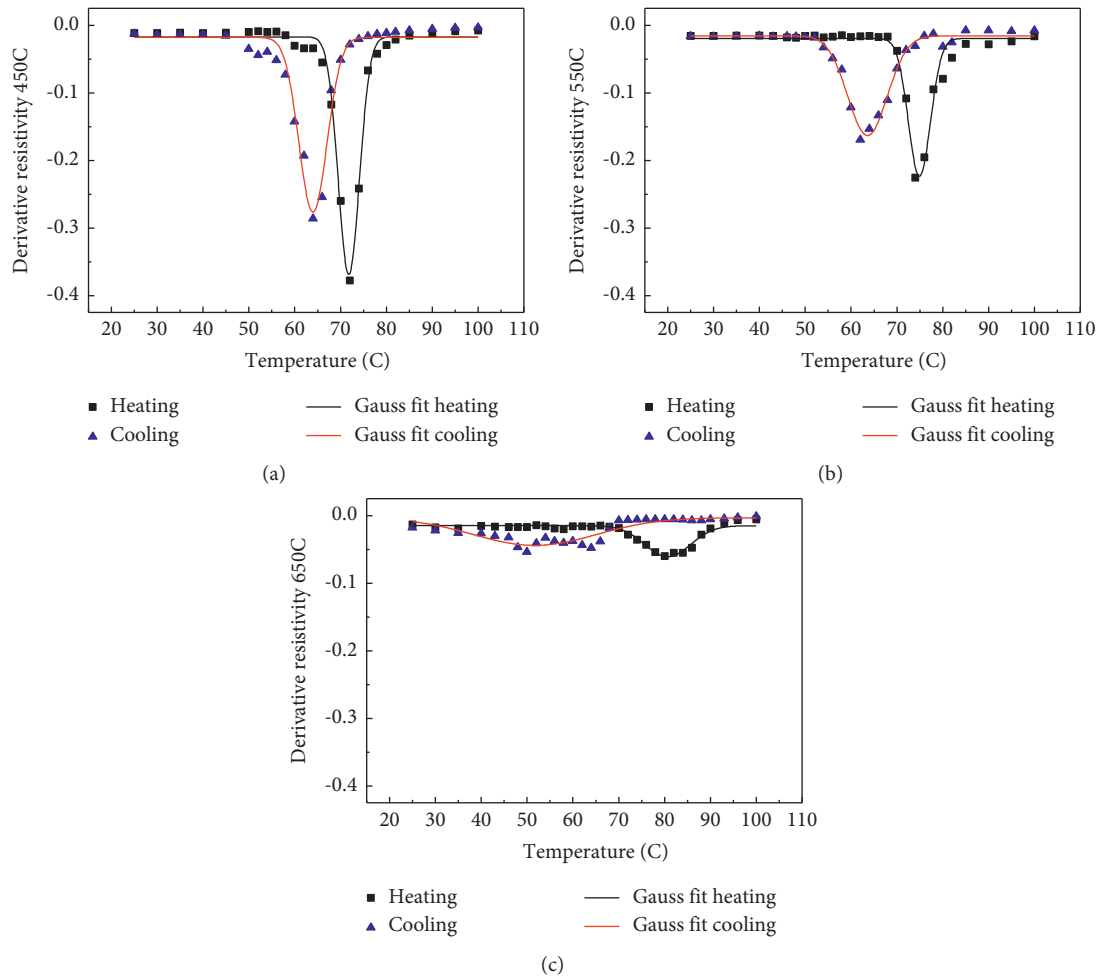
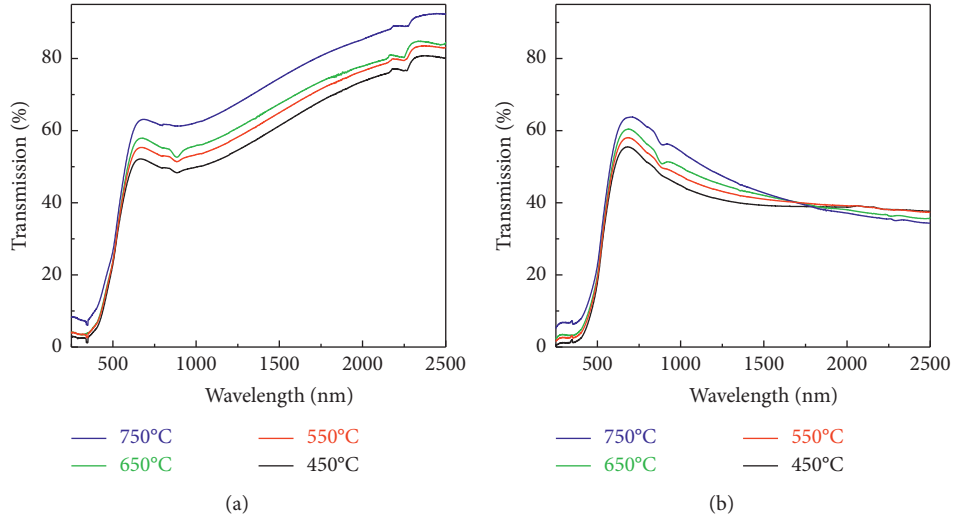


FIGURE 5: Derivative of the resistivity versus temperature of the PLD VO<sub>2</sub>(M) films and the related fit of the results using a Gaussian: (a) 450°C, (b) 550°C, and (c) 650°C.

TABLE 1: The characteristics of the IMT of the PLD VO<sub>2</sub>(M) films grown at different temperatures.

Substrate temperature (°C)	$\Delta R$ (orders of magnitude)	$T_{\text{IMT}}$ (°C)	$\Delta H$ (°C)	$\Delta T$ (°C)	
				Heating	Cooling
450	3.184	72	8	5	7
550	2.718	75	11	6	10.
650	1.705	81	29	12	32

FIGURE 6: Spectral transmittance at room temperature (a) and at 90°C (b) of PLD VO<sub>2</sub>(M) films grown at different temperatures.

applications, such as doping, multilayer films, core-shell nanostructures, and patterning [28]. The main target is to improve the luminous transmittance along with achieving good IR transmittance modulation across  $T_{\text{IMT}}$ . Despite the achieved promising results, the proposed approaches involve complicated synthesis and/or fabrication procedures that may severely limit practical application.

The spectral transmittance measured at room temperature presented in Figure 6(a) shows an enhancement when the substrate temperature of VO<sub>2</sub>(M) films increases. VO<sub>2</sub>(M) layer displays a more open structure when the substrate temperature increases (cf. Figure 3). The medium made of VO<sub>2</sub>(M) and pores will have a lower refractive index, which results in an increase in the transmittance with the porosity [29]. As a result, the integral luminous transmittance at room temperature  $T_{\text{lum,RT}}$  increases from 38.4% for VO<sub>2</sub>(M) film deposited at 450°C to 44.6% for the micro/nanowire VO<sub>2</sub>(M) sample deposited at 750°C (cf. Table 2). This represents a relative increase in  $T_{\text{lum,RT}}$  by 16.1%. The spectral transmittance measured at 90°C is presented in Figure 6(b). Similarly to the trend observed at room temperature, the integral luminous transmittance at 90°C  $T_{\text{lum,90°C}}$  increases from 37.2% for VO<sub>2</sub>(M) film deposited at 450°C to 43.0% for the micro/nanowire VO<sub>2</sub>(M) sample deposited at 750°C (cf. Table 2). This represents a relative increase in  $T_{\text{lum,90°C}}$  by 15.6%. It is important to highlight the fact that  $T_{\text{lum}}$  values are very similar at both room temperature (RT) and 90°C, which means that the visible luminosity remains very stable across the IMT critical temperature. This factor might be very convenient for smart

TABLE 2: Optical properties of the PLD VO<sub>2</sub>(M) films grown at different temperatures.

Substrate temperature (°C)	$T_{\text{lum}}$ (%)		$T_{\text{IR}}$ (%)		$\Delta T_{\text{IR}}$ (%)
	RT	90°C	RT	90°C	
450	38.4	37.2	55.7	43.0	12.7
550	40.1	38.9	59.1	45.1	14
650	41.1	40.1	61.2	46.5	14.7
750	44.6	43.0	68.3	49.4	18.9

windows applications since the objective is to have a stable visible luminosity while ensuring a good modulation of the transmittance in the IR.

The IR transmittance modulation  $\Delta T_{\text{IR}}$  is observed to increase from 12.7% for VO<sub>2</sub>(M) film deposited at 450°C to 18.9% for the micro/nanowire VO<sub>2</sub>(M) sample deposited at 750°C (cf. Table 2). By correlating these results to the decrease in the FWHM (cf. inset in Figure 2), the improvement in the modulation properties can be explained by the improvement in the crystallinity of VO<sub>2</sub>(M) with increasing the temperature [30].

#### 4. Conclusion

VO<sub>2</sub>(M) films with different morphologies were directly grown on smooth fused quartz substrates by a simple PLD approach at a low deposition rate without posttreatment. It was found that the increase in the substrate's temperature not only results in an enhancement of the adatoms diffusion, but also increases the V<sup>5+</sup> state content, resulting in a further

improvement of bulk diffusion due to the low melting point of vanadium oxides containing  $V^{5+}$  valence state. As a result, XRD revealed better (011) texturization and improved crystallinity with increasing the temperature from 450°C to 750°C. In addition, the morphology the  $VO_2(M)$  grains evolved from small-grained, closely packed structure at 450°C, to less packed micro/nanowires structure at 750°C. Resistivity variation as a function of temperature revealed that  $VO_2(M)$  films obtained at low substrate temperature display low insulator-to-metal transition temperature ( $T_{IMT}$ ), large resistivity variation ( $\Delta R$ ), narrow hysteresis width ( $\Delta H$ ), sharp transition, and symmetric hysteresis loop. Increasing substrate temperature resulted in  $VO_2$  films with high  $T_{IMT}$ , low  $\Delta R$ , broad  $\Delta H$ , smooth transition, and asymmetric hysteresis loop. These results were correlated to the composition/microstructure/morphology of the samples. In summary, these results are expected to help in tailoring the resistivity transition toward specific applications of the films such as ultrafast electronic switching devices and memristors.

In terms of optical properties of the  $VO_2(M)$  samples, it was found that an increase in the processing temperature from 450°C to 750°C resulted in an improvement of their luminous transmittance because of the increase in the porosity of the films. On the other hand, the improvement of the crystallinity of  $VO_2(M)$  grains results in an enhancement of the IMT modulation of the transmittance. In summary, the proposed approach allowed achieving a  $VO_2(M)$  film in the form of micro/nanowires with  $T_{lum,RT} = 44.6\%$ ,  $T_{lum,90^\circ C} = 43.0\%$ , and  $\Delta T_{IR} = 18.9\%$ . This combination of properties is promising for smart windows applications. We anticipate that further improvement could be possible through the optimization of micro/nanowires yield and size distribution. Also, it would be interesting to investigate the effect of dopants on  $VO_2(M)$  micro/nanowires to have a synergetic approach for further enhancement of both luminous transmittance and IR modulation ability.

## Data Availability

Data are available on request from the author.

## Conflicts of Interest

The author declares no that there are conflicts of interest.

## Acknowledgments

This work was supported by the Alfaisal University Office of Research and Graduate Studies (IRG project 21417). The author is grateful for the continuous support.

## Supplementary Materials

Figure S1: SEM images of the PLD  $VO_2(M)$  films grown at 650°C and different laser pulsing frequencies: (a) 20 Hz, (b) 14 Hz, (c) 8 Hz, and (d) 2 Hz. Figure S2: XPS spectra of the  $V2p_{3/2}$  peak deconvoluted into  $V^{5+}$ ,  $V^{4+}$ , and  $V^{2+}$ , for the samples processed at different substrate temperatures: (a)

450°C, (b) 550°C, (c) 650°C, and (d) 750°C. (*Supplementary Materials*)

## References

- [1] F. J. Morin, "Oxides which show a metal-to-insulator transition at the neel temperature," *Physical Review Letters*, vol. 3, no. 1, pp. 34–36, 1959.
- [2] A. Hendaoui, N. Émond, S. Dorval, M. Chaker, and E. Haddad, " $VO_2$ -based smart coatings with improved emittance-switching properties for an energy-efficient near room-temperature thermal control of spacecrafts," *Solar Energy Materials and Solar Cells*, vol. 117, pp. 494–498, 2013.
- [3] V. R. Morrison, R. P. Chatelain, K. L. Tiwari et al., "A photoinduced metal-like phase of monoclinic  $VO_2$  revealed by ultrafast electron diffraction," *Science*, vol. 346, no. 6208, pp. 445–448, 2014.
- [4] J. Narayan and V. M. Bhosle, "Phase transition and critical issues in structure-property correlations of vanadium oxide," *Journal of Applied Physics*, vol. 100, Article ID 103254, 2006.
- [5] N. Émond, A. Hendaoui, A. Ibrahim, I. Al-Naib, T. Ozaki, and M. Chaker, "Transmission of reactive pulsed laser deposited  $VO_2$  films in the THz domain," *Applied Surface Science*, vol. 379, pp. 377–383, 2016.
- [6] D. P. Partlow, S. R. Gurkovich, K. C. Radford, and L. J. Denes, "Switchable vanadium oxide films by a sol-gel process," *Journal of Applied Physics*, vol. 70, no. 1, pp. 443–452, 1991.
- [7] M. B. Sahanna, M. S. Dharmaparakash, and S. A. Shivashankar, *Mass Spectrometry Basics*, vol. 12, pp. 333–338, 2002.
- [8] S. Mathur, T. Ruegamer, N. Donia, and H. Shen, "Functional metal oxide coatings by molecule-based thermal and plasma chemical vapor deposition techniques," *Journal of Nanoscience and Nanotechnology*, vol. 8, no. 5, pp. 2597–2603, 2008.
- [9] A. S. Kuzanyan and A. A. Kuzanyan, *Pulsed Laser Deposition of Large-Area Thin Films and Coatings*, IntechOpen, London, UK, 2016.
- [10] S. Lafane, S. Abdelli-Messaci, M. Kechouane et al., "Direct growth of  $VO_2$  nanoplatelets on glass and silicon by pulsed laser deposition through substrate temperature control," *Thin Solid Films*, vol. 632, pp. 119–127, 2017.
- [11] S. Löffler, E. Auer, M. Weil, A. Lugstein, and E. Bertagnolli, "Impact of growth temperature on the crystal habits, forms and structures of  $VO_2$  nanocrystals," *Applied Physics A*, vol. 102, no. 1, pp. 201–204, 2011.
- [12] I. S. Kim and L. J. Lauhon, "Increased yield and uniformity of vanadium dioxide nanobeam growth via two-step physical vapor transport process," *Crystal Growth & Design*, vol. 12, no. 3, pp. 1383–1387, 2012.
- [13] C. Cheng, K. Liu, B. Xiang, J. Suh, and J. Wu, "Ultra-long, free-standing, single-crystalline vanadium dioxide micro/nanowires grown by simple thermal evaporation," *Applied Physics Letters*, vol. 100, no. 10, Article ID 103111, 2012.
- [14] C. Cheng, H. Guo, A. Ammini et al., "Self-assembly and horizontal orientation growth of  $VO_2$  nanowires," *Scientific Reports*, vol. 4, no. 1, p. 5456, 2014.
- [15] "ASTM G173-03 standard tables of reference solar spectral irradiances: direct normal and hemispherical on a 37 degree tilted surface," 2020, <https://www.nrel.gov/grid/solar-resource/spectra-am1.5.html>.
- [16] The Centre for International Economics, "Physiologically-relevant luminous efficiency function for photopic vision," 2008, [http://www.cvrl.org/database/data/lum/linCIE2008v2e\\_1.csv](http://www.cvrl.org/database/data/lum/linCIE2008v2e_1.csv).
- [17] K. Appavoo, D. Y. Lei, Y. Sonnefraud et al., "Role of defects in the phase transition of  $VO_2$  nanoparticles probed by plasmon

- resonance spectroscopy,” *Nano Letters*, vol. 12, no. 2, pp. 780–786, 2012.
- [18] E. Strelcov, A. V. Davydov, U. Lanke, C. Watts, and A. Kolmakov, “In situ monitoring of the growth, intermediate phase transformations and templating of single crystal VO<sub>2</sub> nanowires and nanoplatelets,” *ACS Nano*, vol. 5, no. 4, pp. 3373–3384, 2011.
- [19] J. A. Thornton, “High rate thick film growth,” *Annual Review of Materials Science*, vol. 7, no. 1, pp. 239–260, 1977.
- [20] R. Eason, *Pulsed Laser Deposition of Thin Films Applications-Led Growth of Functional Materials*, Wiley-Interscience, Hoboken, NJ, USA, 2007.
- [21] Y. Zhao, C. Chen, X. Pan et al., “Tuning the properties of VO<sub>2</sub> thin films through growth temperature for infrared and terahertz modulation applications,” *Journal of Applied Physics*, vol. 114, no. 11, Article ID 113509, 2013.
- [22] J. Y. Suh, R. Lopez, L. C. Feldman, and R. F. Haglund Jr., “Semiconductor to metal phase transition in the nucleation and growth of VO<sub>2</sub> nanoparticles and thin films,” *Journal of Applied Physics*, vol. 96, no. 2, pp. 1209–1213, 2004.
- [23] P. Jin, K. Yoshimura, and S. Tanemura, “Dependence of microstructure and thermochromism on substrate temperature for sputter-deposited VO<sub>2</sub> epitaxial films,” *Journal of Vacuum Science & Technology A: Vacuum, Surfaces, and Films*, vol. 15, no. 3, pp. 1113–1117, 1997.
- [24] R. Lopez, L. C. Feldman, and R. F. Haglund Jr., “Size-dependent optical properties of VO<sub>2</sub> nanoparticle arrays,” *Physical Review Letters*, vol. 93, no. 17, Article ID 177403, 2004.
- [25] S. Lysenko, V. Vikhnin, A. Rua, F. Fernandez, and H. Liu, “Critical behavior and size effects in light-induced transition of nanostructured VO<sub>2</sub> films,” *Physical Review B: Condensed Matter*, vol. 82, Article ID 205425, 2010.
- [26] R. Lopez, T. E. Haynes, L. A. Boatner, L. C. Feldman, and R. F. Haglund Jr., “Size effects in the structural phase transition of VO<sub>2</sub> nanoparticles,” *Physical Review B*, vol. 65, no. 22, Article ID 224113, 2002.
- [27] W. Fan, J. Cao, J. Seidel et al., “Large kinetic asymmetry in the metal-insulator transition nucleated at localized and extended defects,” *Physical Review B*, vol. 83, no. 23, Article ID 235102, 2011.
- [28] Y. Cui, Y. Ke, C. Liu et al., “Thermochromic VO<sub>2</sub> for energy-efficient smart windows,” *Joule*, vol. 2, no. 9, pp. 1707–1746, 2018.
- [29] S. Long, X. Cao, Y. Wang et al., “Karst landform-like VO<sub>2</sub> single layer solution: controllable morphology and excellent optical performance for smart glazing applications,” *Solar Energy Materials and Solar Cells*, vol. 209, p. 110449, 2020.
- [30] C. Kang, C. Zhang, Y. Yao et al., “Enhanced thermochromic properties of vanadium dioxide (VO<sub>2</sub>)/glass heterostructure by inserting a Zr-based thin film metallic glasses (Cu<sub>50</sub>Zr<sub>50</sub>) buffer layer,” *Applied Sciences*, vol. 8, no. 10, p. 1751, 2018.